Electrocatalytic activity of AuCeO$_2$/C towards ethylene glycol oxidation and oxygen reduction reactions

Virginija Kepenienė[1*],

Raminta Stagniūnaitė[1],

Daina Upskuvienė[1],

Loreta Tamašauskaitė-Tamašiūnaitė[1],

Vidas Pakštas[1],

Audrius Drabavičius[1],

Mindaugas Andrulevičius[2],

Eugenijus Norkus[1]

[1] *Department of Catalysis,*
Center for Physical Sciences
and Technology,
3 Saulėtekio Avenue,
10257 Vilnius, Lithuania

[2] *Institute of Materials Science*
of Kaunas University
of Technology, 59 Baršausko Street,
50131 Kaunas, Lithuania

AuCeO$_2$/C and Au/C catalysts were obtained by adsorption of AuNPs on the CeO$_2$/C and pure carbon (C) substrates from an Au colloidal solution. It has been found that AuNPs of ca. 50 nm in size were adsorbed on the surfaces of CeO$_2$/C and C; however, electrocatalytic activity of the investigated AuCeO$_2$/C and Au/C catalysts was different. Ethylene glycol oxidation current density values are ca. 3 times higher on the AuCeO$_2$/C catalyst as compared to those of the bare Au/C catalyst. Moreover, the AuCeO$_2$/C catalyst showed more positive onset potentials, as well as higher current in the mixed-kinetic-diffusion region towards the oxygen reduction reaction in an alkaline medium compared to that of the Au/C catalyst.

Keywords: gold nanoparticles, cerium(IV) oxide, ethylene glycol oxidation, oxygen reduction

INTRODUCTION

Low-temperature polymer electrolyte membrane fuel cells (PEMFCs) are undergoing rapid development for mobile applications and, in particular, for the transport sector [1]. Different fuels have been used for fuel cells, whereas hydrogen, methanol and ethanol have been mostly explored. The operation of PEMFCs is based on the oxidation of fuel at the anode and the oxygen reduction reaction (ORR) at the cathode. In the case of direct methanol, ethanol or ethylene glycol (EG) fuel cells (DMFC, DEFC or DEGFC), acidic or alkaline alcohols solutions can be used as fuel. However, oxidation of fuels like alcohols in an alkaline medium is higher than in an acidic one. Moreover, PEMFCs that used an alkaline alcohols solution as fuel are more attractive and less polluted in comparison with the ones that used an acidic solution as fuel [2–4]. Forasmuch, oxidation reactions of ethanol, methanol or EG in an alkaline medium as well as the ORR have drawn increasing interest

*Corresponding author. Email: virginija.kepeniene@ftmc.lt

with the aim to develop active catalysts for DMFC, DEFC or DEGFC in an alkaline medium.

Application of DMFC is widely investigated, but problems such as the low methanol electro-oxidation kinetics and methanol permeation across the proton exchange membrane obstruct its commercialization [1, 5]. Although ethanol has been recognized as the most suitable fuel for the alkaline fuel cell, however, usually the main products of the oxidation of ethanol on Au at the lower temperatures are acetaldehyde and acetic acid, which complicate to get the clean catalytic process [6–8]. In this case, as the actual and theoretical electron transfer numbers per one ethanol molecule are 4 and 12 for partial oxidation of ethanol to acetic acid and complete oxidation of ethanol to carbon dioxide, respectively, the electron transfer rate (ETR) of ethanol in the alkaline DEFC is only 33% [8]. EG has been found as another choice for alkaline fuel cells. It was determined that the ETR of EG in the alkaline DEGFC is ca. 80%. This value is much higher than that in the alkaline DEFC. In addition, EG owns many remarkable advantages including low toxicity, favourable storage, ease of transport and production from biomass and industry [8–10].

In order to improve the performance of fuel cells, it is very important to develop effective and selective catalysts for fuel oxidation and ORR. Au has been investigated as an excellent catalyst in an alkaline medium [5, 11–14]. Comparing peculiarities of the application of Au and platinum (Pt) for the oxidation reaction of alcohols in an alkaline medium, a higher oxidation activity shows Au as compared with that for Pt. This can be explained by the resistance of the Au surface to the poisoning by intermediates, which are formed during the oxidation of alcohol [2, 14]. Ureta-Zanartu et al. compared activity of Au for methanol and EG oxidation reactions and explored that EG is oxidized at a higher rate [13]. Au has been found to be the best catalyst for the oxidation of EG owing to the fact that EG adsorbs strongly onto the surface of Au [15–21]. The highly dispersed Au particles on the metal oxides supports, including Co_3O_4, SnO_x, MnO_2, RuO_2, etc., exhibit an extraordinarily high activity for the oxidation reaction of various materials at low temperatures [22–26] as well as for ORR [27, 28]. Cerium(IV) oxide (CeO_2) is an attractive co-catalyst for various noble metals

due to its oxygen vacancy, i.e. oxygen storage capacity ability, functioning as an oxygen buffer by storing/releasing O_2 due to the Ce^{4+}/Ce^{3+} redox couple. This results in supplying sufficient OH_{ads} at low potential values and the efficient eliminating of poisoning intermediates during the reaction. Other positive properties of CeO_2, such as low price, synergistic effect between CeO_2 and metal as well as tolerance to the CO poisoning, determine the choice of this oxide as an additive in the preparation of various catalysts [22, 29, 30]. CeO_2 is widely used for combining it with Pt, Pd or other oxides [31–33]. However, nanosized Au particles supported on metal oxides have been extensively studied because of their high reactivity in a variety of important catalytic reactions. Although, the interaction between Au and CeO_2 is not widely described, the combination of CeO_2 and Au may lead to the formation of materials that have an enhanced electrocatalytic activity for the ORR and EG oxidation [13, 22].

In the paper presented herein, we investigated the electrocatalytic activity of $AuCeO_2/C$ and Au/C catalysts prepared by the adsorption of AuNPs on the CeO_2/C and C substrates from an Au colloidal solution. The composition, morphology and structure of the prepared catalysts have been characterized using inductively coupled plasma optical emission spectroscopy (ICP-OES), field emission scanning electron microscopy (FESEM), transmission electron microscopy (TEM), X-ray photoelectron spectroscopy (XPS) and X-ray diffraction (XRD). Electrocatalytical properties of the prepared $AuCeO_2/C$ and Au/C catalysts have been investigated towards the oxidation of EG in an alkaline medium using cyclic voltammetry (CV), whereas the reduction of oxygen has been investigated by means of linear sweep voltammetry (LSV) using the rotating disk electrode (RDE) method.

It has been found that the $AuCeO_2/C$ catalyst showed an enhanced electrocatalytic activity towards the oxidation of EG and ORR in an alkaline medium compared to the bare Au/C catalyst.

EXPERIMENTAL

Chemicals
$HAuCl_4$ (99.995%), CeO_2 powder (99.9%) and carbon powder (99.999%) were purchased from

Sigma-Aldrich and Alfa-Aesar Supplies. Polyvinylidenefluoride (PVDF), N-methyl-2-pyrrolydone (NMP), ethylene glycol $(CH_2OH)_2$, ethanol (96%), H_2SO_4 (96%), glucose (99.5%), ascorbic acid (99%) and NaOH (98.8%) were purchased from Chempur Company. Oxygen gas (99.999%) was used for the saturation of the NaOH solution. Pt/C wt. 46.4% Pt (TEC10E50E) was purchased from Tanaka Kikinzoku Kogyo K. K. Supplier. All chemicals were of analytical grade. Ultra-pure water with a resistivity of 18.2 MΩ cm⁻¹ was used for preparing the solutions.

Preparation of catalysts
For the formation of the $AuCeO_2$/C catalyst, at first, CeO_2/C substrate was prepared and further AuNPs were deposited on the CeO_2/C surface from the Au colloidal solution. The CeO_2/C substrate was prepared by the following procedure: dry CeO_2 powder was mixed with carbon powder (mass ratio being 1:1) in a 2-propanol solution by ultrasonication for 30 min with further drying of the obtained mixture. The Au colloidal solution was prepared by adding 1 ml of the solution containing 0.1 M glucose and 0.05 M ascorbic acid to 30 ml of the 0.3 mM $HAuCl_4$ solution. The solution quickly got cherry red colour indicating reducing of Au^{3+} to Au^0. Then, for the preparation of the $AuCeO_2$/C catalyst, 100 mg of the prepared CeO_2/C powder was added to the obtained Au colloidal solution. The mixture was stirred for 1 h until the solution became transparent. The obtained $AuCeO_2$/C catalyst powder was filtered and dried in a vacuum oven at 80°C temperature for 2 h. The Au/C catalyst was prepared in the same manner by using 100 mg of pure carbon powder instead of CeO_2/C.

Characterization of catalysts
XRD patterns of the studied $AuCeO_2$/C and Au/C powders were measured using an X-ray diffractometer SmartLab (Rigaku) equipped with an X-ray tube with a 9 kW rotating Cu anode. The measurements were performed using Bragg–Brentano geometry with a graphite monochromator on a diffracted beam and a step scan mode with a step size of 0.02° (in 2θ scale) and counting time of 1s per step. The measurements were conducted in a 2θ range of 20–70°. Phase identification was performed using the software package

PDXL (Rigaku) and the ICDD powder diffraction data base PDF4+ (2018 release). The size of crystallites was calculated from XRD peaks broadening using the graphical Halder–Wagner method in the PDXL software.

A shape and size of AuNPs were examined using a transmission electron microscope Tecnai G2 F20 X-TWIN equipped with an EDAX spectrometer with an r-TEM detector. For microscopic examinations, 10 mg of the sample was first sonicated in 1 ml of ethanol for 1 h and then the obtained mixture was deposited on the Cu grid covered with a continuous carbon film.

The morphology and composition of the fabricated catalysts were characterized using a SEM/FIB workstation Helios Nanolab 650 with an energy dispersive X-ray (EDX) spectrometer INCA Energy 350 X-Max 20.

The chemical composition of the prepared catalysts was determined by means of X-ray photoelectron spectroscopy (XPS) using an ESCALAB 250Xi Avantage spectrometer (VG Scientific, UK) equipped with an Al Kα X-ray radiation source (1486.6 eV) and operated at a fixed pass energy of 40 eV. The base pressure in the analytical chamber was better than 8×10^{-7} Pa.

The Au loading in the prepared catalysts was estimated by means of ICP-OES using an ICP optical emission spectrometer Optima 7000DV (Perkin Elmer).

Electrochemical measurements
Electrochemical measurements were assessed using the RDE and the AUTOLAB electrochemical workstation. A three-electrode conventional cell was used, where the glassy carbon RDE with a geometric area of 0.07 cm² was used as the working electrode, a Pt sheet was used as a counter electrode and an Ag/AgCl/KCl$_{sat}$ electrode was used as a reference. The catalysts suspensions were obtained according to the following steps: at first, 10 mg of the $AuCeO_2$/C and Au/C catalysts were dispersed ultrasonically in 100 μl of 2% PVDF in the NMP solution for 1 h. With the aim to keep a similar amount of Au during the measurement, a required amount of the prepared catalyst suspension was pipetted onto the polished surface of a glassy carbon electrode and dried in an oven at 80°C temperature for 4 h.

In order to determine electrochemically active surface areas (ESAs) of AuNPs in the prepared

catalysts, the cyclic voltammograms (CVs) were recorded in a 0.5 M H_2SO_4 solution. The electrode potential was cycled in a range of –0.2–1.4 V with a scan rate of 50 mV s^{-1}. The oxidation of EG in an alkaline medium was investigated by recording CVs in a 1 M $(CH_2OH)_2$ + 0.5 M NaOH solution at a scan rate of 50 mV s^{-1} from –0.3 to 1.1 V. Chronoamperometric measurements (CA) were carried out in the same solution at a constant potential value of 0.5 V for 30 min. The electrode potential values are quoted versus the silver/silver chloride electrode (Ag/AgCl/KCl$_{sat}$).

For ORR measurements, an O_2-saturated 0.1 M NaOH solution was used. Linear sweep voltammetry curves (LSVs) were recorded in the electrode potential range from 1 to 0.2 V in the cathodic direction at a scan rate of 5 mV s^{-1} and varying the rotation speed from 0 to 2000 rpm. CA for ORR were recorded at a potential value of 0.5 V in the O_2-saturated 0.1 M NaOH solution for 30 min. The electrode potential values for ORR are quoted versus the reversible hydrogen electrode (RHE).

Koutecky–Levich (K–L) equations (1–3) were used for calculation of the electron transfer numbers per oxygen molecule (*n*) in ORR:

$$j^{-1} = j_k^{-1} + j_d^{-1}, \tag{1}$$

$$j_d = 0.62 nFD^{2/3} \, Co_2 v^{-1/6} \, \omega^{1/2}, \tag{2}$$

$$j^{-1} = j_k^{-1} + \omega^{-1/2} \times A. \tag{3}$$

Here *j*, j_k and j_d are the measured current density, kinetic current density and the diffusion-limiting current density (mA cm^{-2}), respectively; *n* is the number of electrons transferred in the reaction; F is the Faraday constant (*F* = 96.485 C mol^{-1}); D is the diffusion coefficient of the reactant (1.9 × 10^{-5} cm^2 s^{-1}); Co_2 is the concentration of the reactant in the bulk electrolyte (1.2 × 10^{-3} mol L^{-1}); ν is the kinetic viscosity of the electrolyte (1.13 × 10^{-2} cm^2 s^{-1}); ω is the rotation rate; A is the slope of the linear plot of j^{-1} versus $\omega^{-1/2}$ (K–L plot) [34].

All measurements were carried out at 25°C temperature. All solutions were dearated with Ar before each measurement, except ORR measurements. The presented current densities are normalized with respect to the geometric area of the working electrode.

RESULTS AND DISCUSSION

Figure 1 presents the XRD profiles of the Au/C (pattern a) and AuCeO$_2$/C (pattern b) catalysts. As evident, the XRD pattern of the Au/C catalyst shows diffraction peaks at 2θ = 38.18, 44.39 and 64.58° which were assigned to the (111), (200), and (220) crystallographic planes of cubic Au phase (ICDD # 00-004-0784). The received Au diffraction peaks are rather broad, which indicates that the Au crystallites are quite small with an average size of 9.8 ± 0.5 nm (Fig. 1, pattern a). In the case of AuCeO$_2$/C (Fig. 1, pattern b), the obtained diffraction peaks were assigned to the same crystallographic planes of cubic Au phase at the same 2θ values. The characteristic diffraction peaks obtained at 2θ = 28.58, 33.12, 47.54 and 56.41° were assigned to the (111), (200), (220) and (311) crystallographic planes of cubic CeO$_2$ phase (ICDD # 00-034-0394) (Fig. 1, pattern b). The Au and CeO$_2$ crystallites ca. 4.5 ± 0.4 nm and ca. 16.2 ± 0.6 nm in size, respectively, were estimated in the AuCeO$_2$/C catalyst. The theoretical cubic Au lattice constant A is 4.0786 Å, while that of CeO$_2$ is 5.4113 Å. For both Au/C and AuCeO$_2$/C catalysts, no changes in the lattice parameters for Au and CeO$_2$ were observed. Therefore, it can be assumed that solid solutions did not form in the synthesized AuCeO$_2$/C catalyst. However, the size of Au crystallites in the AuCeO$_2$/C catalyst was approximately 2-fold smaller than those in the pure Au/C catalyst.

X-ray photoelectron spectroscopy was used for the determination of surface elemental composition and chemical state of the prepared catalysts.
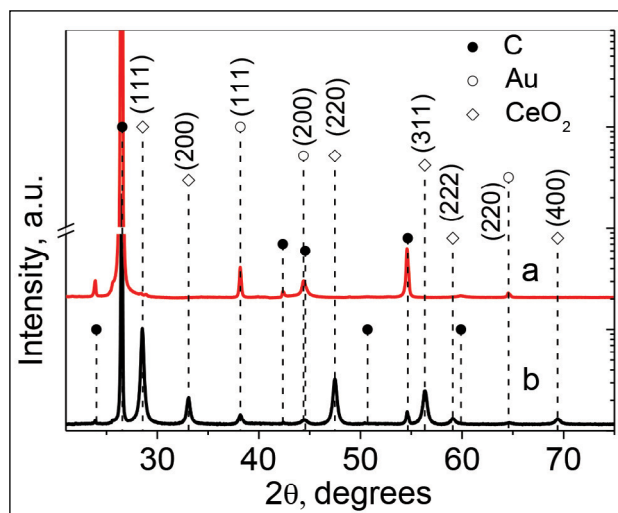

Fig. 1. XRD patterns of the Au/C (a) and AuCeO$_2$/C (b) catalysts

The XPS spectra of the Au 4f, O 1s, Ce 3d and C 1s regions for AuCeO$_2$/C and Au/C are given in Fig. 2. The binding energy values (BEs) of spin-orbital splitting peaks are listed in Table 1. The Au4f XPS spectra of the Au/C and AuCeO$_2$/C catalysts showed doublets assigned to the 4f$_{7/2}$ and 4f$_{5/2}$ phases for metallic Au with binding energy differences of 4.03 and 3.6 eV, respectively (Fig. 2a) [35, 36]. For the O 1s XPS spectra, the BE peak at 532.22 eV was attrib-

uted to the presence of the surface of adsorbed O$_2$, H$_2$O or CO$_2$ for both Au/C and AuCeO$_2$/C catalysts (Fig. 2b) [37]. The BE peak at 529.62 eV in the O 1s spectrum for the AuCeO$_2$/C catalyst was assigned to lattice oxygen species (Fig. 2b, a dashed line) [37]. The Ce 3d spin-orbital splitting peaks were attributed to the 3d$_{5/2}$ and 3d$_{3/2}$ transitions of Ce, which correspond to Ce^{4+} (Fig. 2c, Table 1) [38, 39]. Figure 2 d shows XPS spectra of the C 1s region with
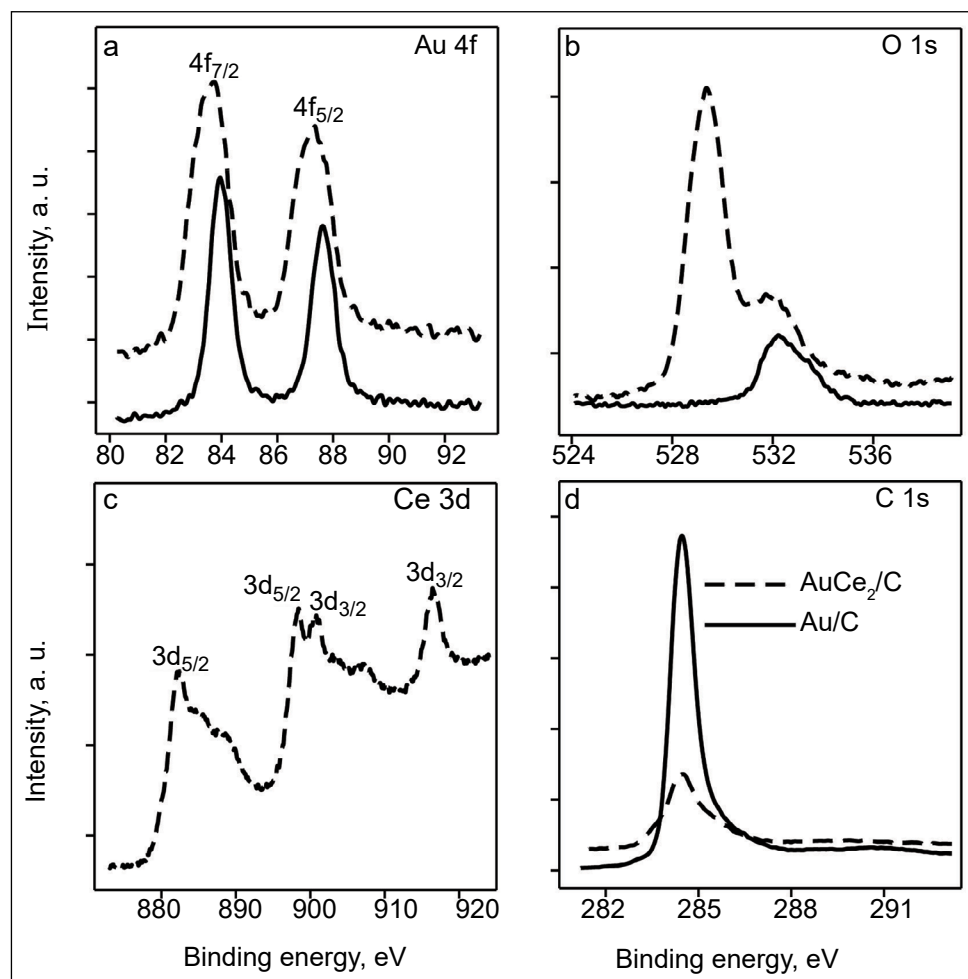

Fig. 2. XPS spectra of the Au 4f (a), O 1s (b), Ce 3d (c) and C 1s (d) regions for the Au/C (a solid line) and AuCeO$_2$/C (a dashed line) catalysts

Table 1. XPS analysis of the elemental composition of catalysts

Sample	Au 4f		Ce 3d		O 1s		C 1s	
	E_b, eV	at.%	E_b, eV	at.%	E_b, eV	at.%	E_b, eV	at.%
AuCeO$_2$/C	87.36	0.60	916.40	9.96	532.22	27.38	284.49	62.06
	83.76		907.20		529.62			
			898.41					
			882.41					
Au/C	87.99	0.19	–	–	532.22	3.07	284.49	96.73
	83.96							

a spin-orbital splitting peak at 284.49 eV, which is assigned to carbon [40, 41].

In order to evaluate the size and shape of AuNPs in the prepared catalysts, TEM analysis was carried out (Fig. 3). It is clearly seen that spherical AuNPs were deposited on the surfaces of CeO_2/C (Fig. 3a) and carbon (Fig. 3b). The size of AuNPs is ca. 40–50 nm in both prepared catalysts. SEM images of the $AuCeO_2/C$ and Au/C catalysts (Fig. 4) confirmed the data obtained by the TEM analysis. It is evident that spherical AuNPs of ca. 50 nm in size were deposited on the CeO_2/C (Fig. 4a) and carbon (Fig. 4b) substrates.

Electrochemically active surface area values of AuNPs in the $AuCeO_2/C$ and Au/C catalysts were determined from CVs recorded in a 0.5 M H_2SO_4 solution (Fig. 5) and by integrating the area of the peak associated with the reduction of AuO at about 1.0 V with a charge density of 400 $\mu C\ cm^{-2}$ [42]. The summarized data are presented in Table 2. The Au loading in the prepared catalysts determined by ICP-OES are also listed in Table 2.

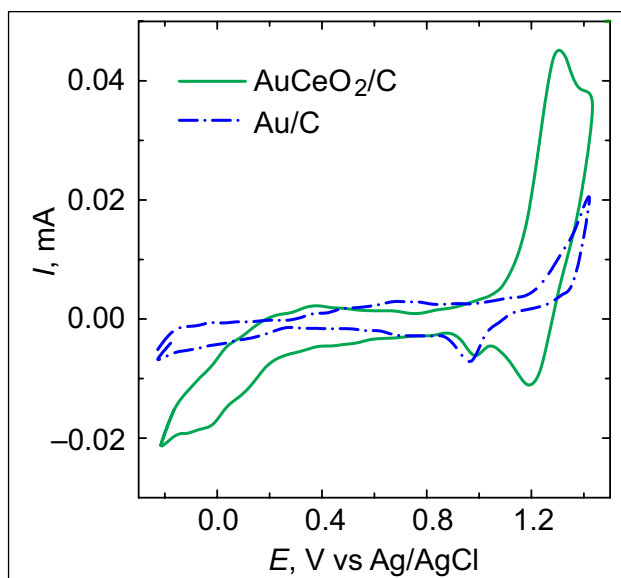**Fig. 5.** CVs of $AuCeO_2/C$ (a solid line) and Au/C (a dashed line) recorded in a 0.5 M H_2SO_4 solution at 50 mV s^{-1}

The electrocatalytic activity of the $AuCeO_2/C$ and Au/C catalysts were examined for the oxidation of EG in an alkaline medium by cyclic voltammetry. Long-term CVs for the investigated
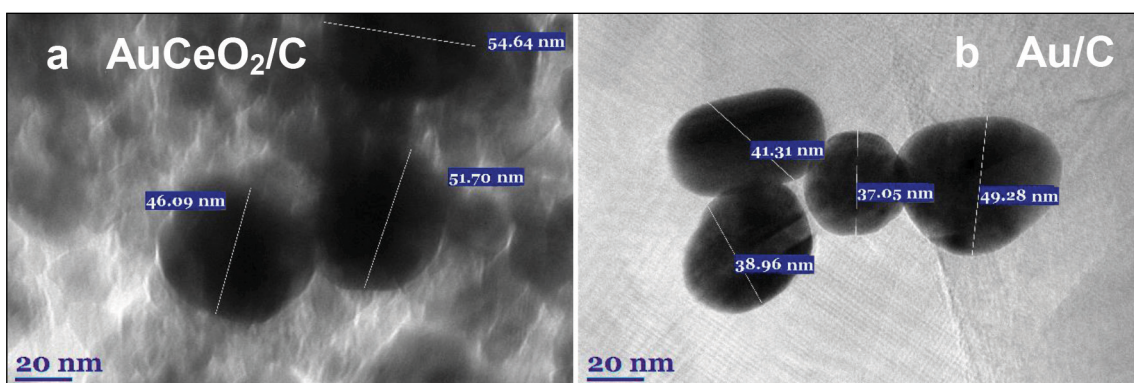

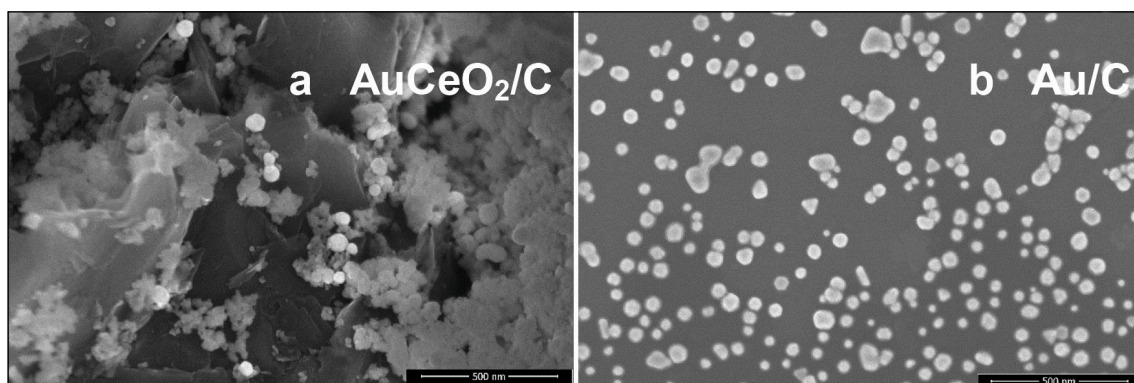**Fig. 3.** TEM images of the $AuCeO_2/C$ (a) and Au/C (b) catalysts

Fig. 4. SEM images of the $AuCeO_2/C$ (a) and Au/C (b) catalysts

catalysts recorded in a 1 M $(CH_2OH)_2$ + 0.5 M NaOH solution at a sweep rate of 50 mV s^{-1} are shown in Fig. 6. As evidence, two anodic current peaks **I** and **II** in the forward and reverse scans,
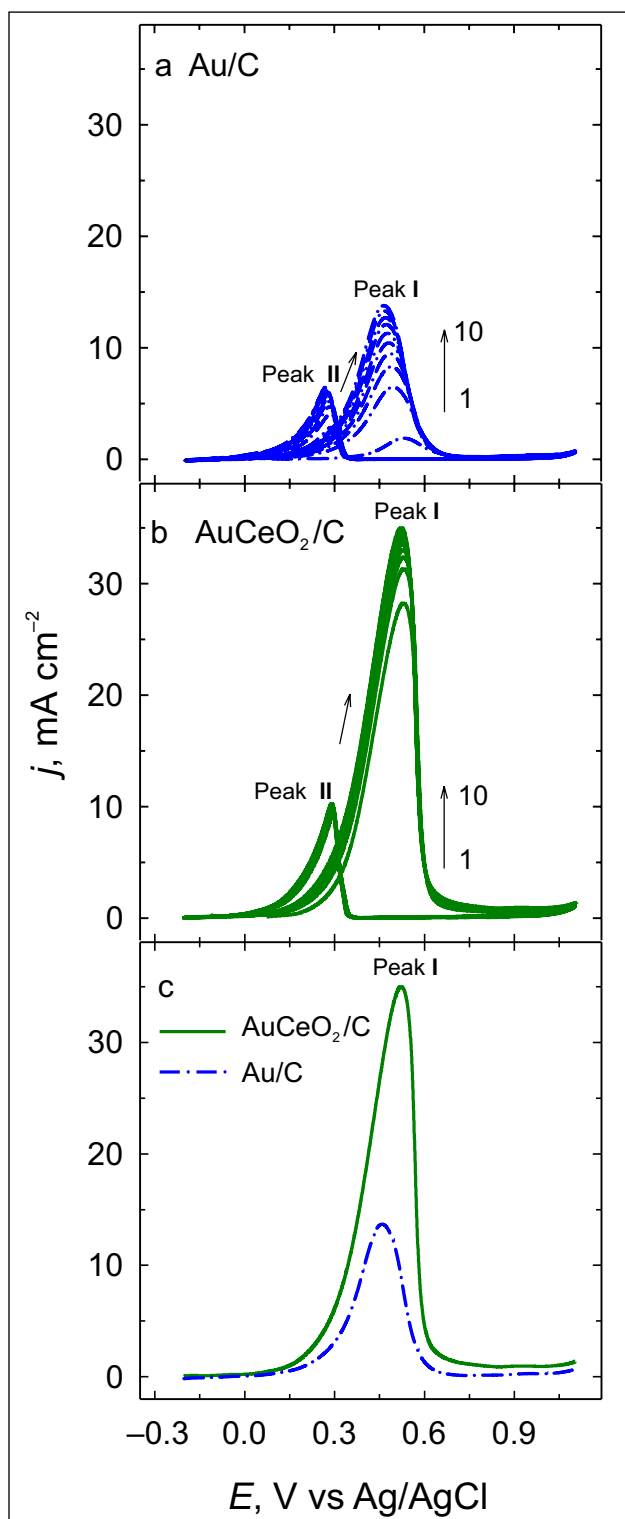

Fig. 6. CVs of the Au/C (a) and AuCeO$_2$/C (b) catalysts recorded in a 1 M (CH$_2$OH)$_2$ + 0.5 M NaOH solution at 50 mV s^{-1}; 25°C. (c) Stabilized positive potential-going scans of the same catalysts at the same conditions

respectively, were recorded at both AuCeO$_2$/C and Au/C catalysts (Fig. 6a, b). These anodic peaks are related to the oxidation reaction of hydrocarbons in the forward scan and with incompletely oxidized carbonaceous residues on the catalyst surface during the reverse scan [43]. The maximum current density of anodic peaks **I** was reached at ca. 0.5 V at both AuCeO$_2$/C and Au/C catalysts, whereas anodic peaks **II** appear at ca. 0.25 V in the reverse scan (Fig. 6a, b). It should be noted that during long-term scanning, EG oxidation current density values corresponded to the peak **I** on both catalysts increase, indicating a high activity and stability of catalysts.

Particular current density values of the anodic peaks of forward (j_F) and reverse (j_R) scans are given in Table 2. The ratio (j_F/j_R) of forward anodic peak current density to the reverse anodic peak expresses an index of the catalysts tolerance to the poisoning species accumulated on the surface of the electrode. For AuCeO$_2$/C and Au/C j_F/j_R ratios were calculated and they are equal to 3.42 and 2.13, respectively. Higher j_F/j_R ratio indicates a more efficient oxidation of EG with a little accumulation of carbonaceous residues during the forward scan [43, 44]. According to the j_F/j_R data, the CeO$_2$ supported AuNPs catalyst shows its better tolerance to the poisoning of carbonaceous residues as compared with that of the carbon supported AuNPs catalyst.

The stabilized positive potential-going scans (10th cycle of scan) of AuCeO$_2$/C and Au/C are presented in Fig. 6c. It was found that the onset potential for the oxidation of EG on the AuCeO$_2$/C catalyst starts at ca. −0.2 V. Moreover, this value is more negative compared to that of the Au/C catalyst, which is ca. −0.1 V. EG oxidation current density that corresponds to the peak **I** is 2.5 times higher at the AuCeO$_2$/C catalyst, compared with that for the bare Au/C catalyst. These results greatly highlighted the enhanced catalytic activity and better stability of the AuCeO$_2$/C catalyst, which may be attributed to the synergistic catalytic effects of AuNPs and CeO$_2$.

Figure 7 illustrates the EG oxidation current densities, which were normalized by the electrochemically active surface areas of AuNPs in the catalysts and the Au loading for each catalyst. The values obtained represent the mass (mA mg$_{Au}^{-1}$) (Fig. 7a) and specific (mA cm^{-2}) (Fig. 7b) activities

Table 2. Electrochemical parameters of the Au/C and AuCeO₂/C catalysts

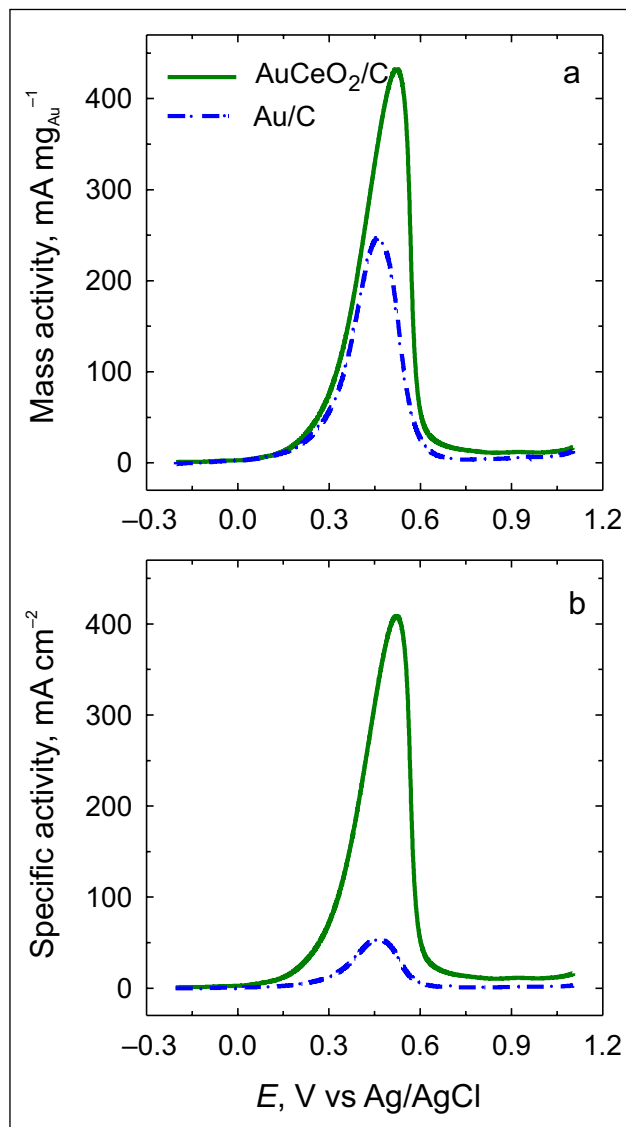| Catalyst	ESA, cm^{-2}	Au loading, μg cm^{-2}	j_F, mA cm^{-2}	j_R, mA cm^{-2}
Au/C	0.018	56.00	13.81	6.47
AuCeO₂/C	0.006	81.00	34.99	10.24

Fig. 7. Comparison of the mass (a) and specific (b) activities towards the oxidation of EG under peaks **I** for AuCeO₂/C and Au/C recorded in 1 M (CH₂OH)₂ + 0.5 M NaOH at 50 mV s^{-1}

of the AuCeO₂/C and Au/C catalysts towards EG oxidation. The mass and specific activities for EG oxidation were ca. 2 and 8 times higher, respectively, at the AuCeO₂/C catalyst compared with those for the Au/C catalyst (Fig. 7a, b).

The electrochemical stability of as-prepared catalysts for the oxidation of EG was investigated using CA (Fig. 8). The potential was firstly held at open circuit for 10 s, then set to 0.5 V for 1900 s

in a 1 M (CH₂OH)₂ + 0.5 M NaOH solution at 25°C. As seen in Fig. 8a, a current density decay was observed at first 5 min. Then it gradually stabilizes and reaches the current density values ca. 5 and 13 mA cm^{-2} for Au/C and AuCeO₂/C, respectively. As evident, the AuCeO₂/C catalyst shows a higher current density at the end of experiment as compared to that at Au/C (Fig. 8a). The mass and specific activity values were calculated from the current densities obtained at the end of the experimental period ($t = 1900$ s) and are given in Fig. 8b and c. It is evident that mass (Fig. 8b) and specific (Fig. 8c) activity values of the AuCeO₂/C catalyst are ca. 2 and 8 times higher as compared to those for Au/C, respectively. These data confirm the results obtained by CV.

The as-prepared Au/C and AuCeO₂/C catalysts were also investigated towards the oxygen reduction reaction. Figures 9a and b show the ORR polarization curves recorded on the investigated catalysts in the O₂-saturated 0.1 M NaOH solution. The electrode potential was scanned in the cathodic direction from 1.0 to 0.2 V at a scan rate of 5 mV s^{-1}. The rotation speed was varied from 400 to 2000 rpm (Fig. 9a, b). From the data obtained, it is seen that AuCeO₂/C and Au/C demonstrate a typical view of ORR curves with the onset potential of ca. 0.80 V. According to the literature data, at potential values between 0.7 and 0.9 V (vs RHE) the ORR response is dominated by the kinetics of electrocatalysts [45]. The Koutecky–Levich plots were obtained from the RDE data on oxygen reduction at potentials from 0.2 up to 0.5 V for both catalysts and are shown in Fig. 9c and d. In general, the K–L curves display a linear relationship between j^{-1} and $w^{-1/2}$ indicating the first-order dependence of the ORR kinetics at different potentials (0.2–0.5 V). According to the K–L equations (1–3), the calculated number of electrons transferred (n) on both Au/C and AuCeO₂/C catalysts was obtained ca. 2.5 (Fig. 9c, d, the insets). This indicates that the both AuCeO₂/C and Au/C catalysts favour a 2-electron transfer reaction path and O₂ is reduced to HO₂$^-$ and OH$^-$ [46, 47].
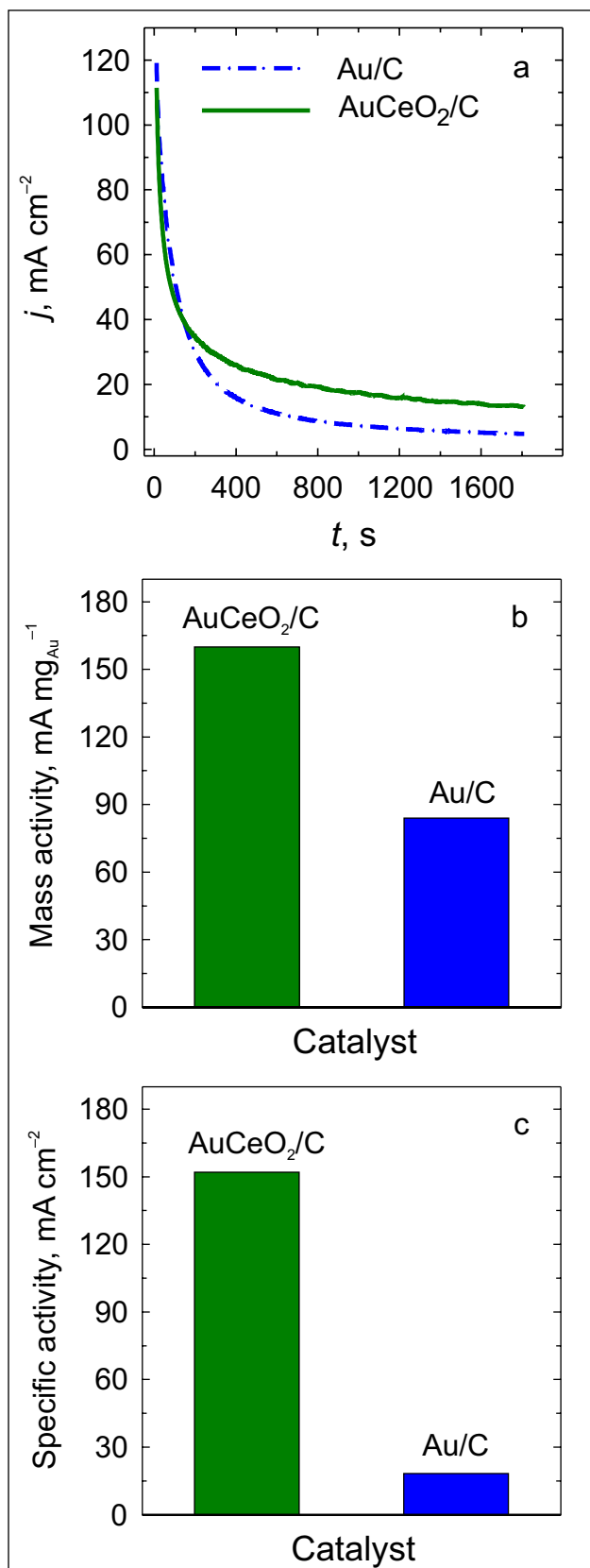
Fig. 8. CA data for AuCeO$_2$/C and Au/C studied in 1 M (CH$_2$OH)$_2$ + 0.5 M NaOH at 0.5 V vs Ag/AgCl for 1900 s. Bar columns of EG oxidation current densities obtained at the end of experimental period and normalized by the Au loading (b) and electrochemically active surface areas of AuNPs (c) for each catalyst

Figure 10a compares the LSV scans of AuCeO$_2$/C, Au/C and the commercial Pt/C catalyst that has the Pt loading of 0.071 mg Pt cm^{-2} at a rotation speed of 1600 rpm. The determined onset potential for Pt/C was equal to 0.95 V. It is clearly seen that the AuCeO$_2$/C onset potential should be more positive compared to that of the Pt/C catalyst. Nevertheless, LSVs display that AuCeO$_2$/C demonstrated higher current density in the mixed-kinetic-diffusion region as compared with that at the Au/C catalyst. It can be assumed that the CeO$_2$ supported AuNPs catalyst shows an enhanced electrocatalytic activity towards the oxygen reduction reaction. The ORR current densities were also normalized by the electrochemically active surface areas of AuNPs and Au loadings for both catalysts at a potential value of 0.75 V at a rotation speed of 1600 rpm (Fig. 10b). As seen from the data obtained, the mass and specific activity is 1.5 and 6 times higher, respectively, at the AuCeO$_2$/C catalyst compared with that at Au/C (Fig. 10b). The data received confirms the synergetic action between present metal and metal oxide in the catalyst composition. Although the mixed-kinetic-diffusion current densities are not low, the onset potential should be at least of 0.1 V more positive for the efficient oxygen reduction reaction. The durability of the prepared Au/C and AuCeO$_2$/C catalysts was evaluated by CA measurements at a potential value of 0.5 V (vs RHE) for 1900s (Fig. 10c). It is seen that after approximately 200 s the current density settled down and only slightly increased with time. Figure 10c' presents the normalized ORR current densities (%) for each catalyst after 200 s. It is seen that the Au/C, AuCeO$_2$/C and commercial Pt/C catalysts maintained 82.2, 78.5 and 80.1%, respectively, of their initial signals. This manifests that the as-synthesized catalysts demonstrated a similar stability to commercial Pt/C during the ORR process in an alkaline medium.

We compared the electrocatalytic activity towards the oxidation of EG and ORR of our prepared catalysts with other Au or CeO$_2$ supported catalysts recently reported in the literature (Table 3). From the data in Table 3, it is seen that the as-prepared AuCeO$_2$/C catalyst exhibits higher electrocatalytic activity towards the ethylene glycol oxidation reaction.
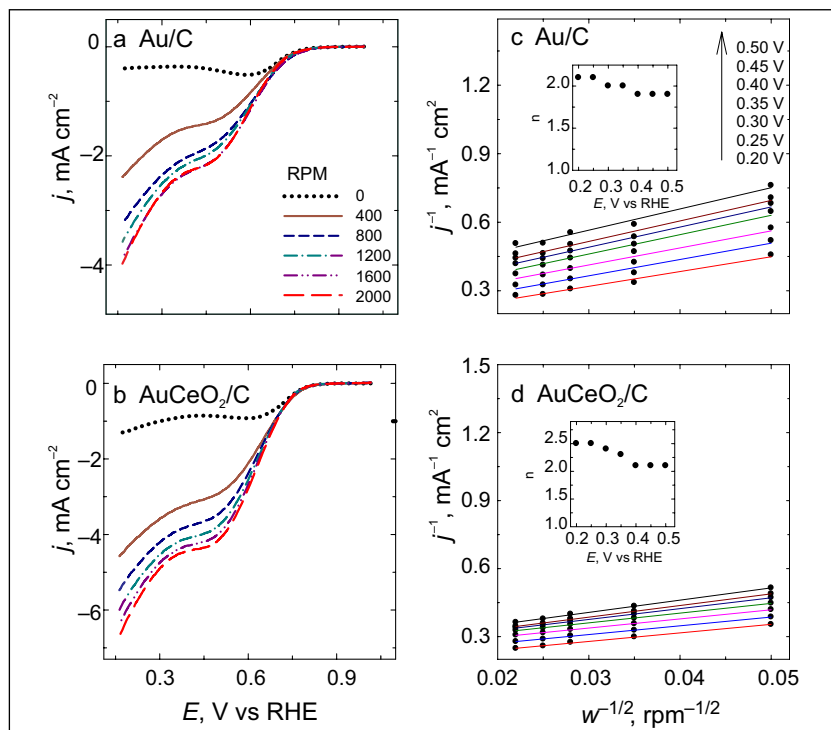
Fig. 9. LSVs of the Au/C (a) and AuCeO$_2$/C (b) catalysts recorded in an O$_2$-saturated 0.1 M NaOH solution at 5 mV s^{-1} and varying the rotation speed from 0 to 2000 rpm. Koutecky–Levich plots of ORR collected for Au/C (c) and AuCeO$_2$/C (d). The insets show the calculated electron transferred number for each catalyst
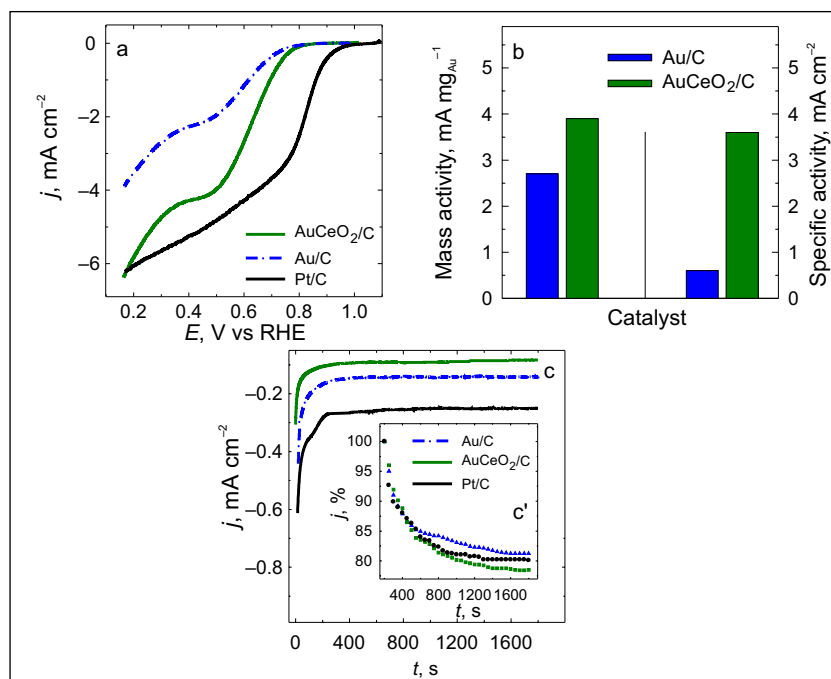

Fig. 10. (a) Comparison of LSVs of the Au/C, AuCeO$_2$/C and commercial Pt/C catalysts recorded in an O$_2$-saturated 0.1 M NaOH solution at 1600 rpm. (b) Bar columns of the ORR mass and specific activities for Au/C and AuCeO$_2$/C calculated from LSVs at 0.75 V. (c) CA data of Au/C, AuCeO$_2$/C and Pt/C recorded in a O$_2$-saturated 0.1 M NaOH solution at 0.5 V vs RHE. Inset c′ represents chronoamperometric responses (percentage of current density retained vs operation time) of all the catalysts

Table 3. The comparison of onset potentials for the ORR and EG oxidation current densities of various catalysts presented in the literature and this study

Catalyst	ORR		EG oxidation		Ref.
	E_{onset}, V vs RHE	Electrolyte	$j_{peak\,l}$, mA cm^{-2}	Electrolyte	
Au/C	0.78	0.1 M NaOH	13.81	0.5 M NaOH + 1 M (CH$_2$OH)$_2$	This study
AuCeO$_2$/C	0.82		34.99		
Pd/Au	0.86	0.1 M NaOH	–	–	[32]
CeO$_2$/MnO$_2$	0.92	0.1 M KOH	–	–	[33]
Au-RGO	0.93	1 M KOH	–	–	[48]
Au nanodendrites	0.88				
Au/RGO	–	–	16.6	0.5 M NaOH + 0.1 M (CH$_2$OH)$_2$	[49]
Au	–	–	6.7	0.5 M NaOH + 0.1 M (CH$_2$OH)$_2$	[50]
PtCeO$_2$ (4:1)/C	–	–	9.8	1 M KOH +1 M (CH$_2$OH)$_2$	[31]
PtCeO$_2$ (2:1)/C	–	–	15.1		
PtCeO$_2$ (1.3:1)/C	–	–	19.2		
PtCeO$_2$ (1:1)/C	–	–	14.7		

CONCLUSIONS

In summary, AuCeO$_2$/C and Au/C catalysts have been prepared by the adsorption of AuNPs on the CeO$_2$/C and pure C substrates from an Au colloidal solution. The oxidation of ethylene glycol and the reduction of oxygen have been investigated in an alkaline medium.

The obtained results suggest that the AuCeO$_2$/C catalyst showed ca. 3 times enhanced electrocatalytic activity towards the oxidation of ethylene glycol compared to that of Au/C. Moreover, AuCeO$_2$/C showed a more positive onset potential, as well as higher current density in the mixed-kinetic-diffusion region towards ORR in an alkaline medium compared to that at the bare Au/C catalyst. The enhanced electrocatalytic activity of AuCeO$_2$/C catalyst should be attributed to the synergistic catalytic effects of AuNPs and CeO$_2$.

References

1. E. Antolini, E. R. Gonzalez, *J. Power Sources*, **195**, 3431 (2010).
2. P. Quaino, N. B. Luque, R. Nazmutdinov, E. Santos, W. Schmickler, *Angew. Chem. Int.*, **51**, 12997 (2012).
3. K. Matsuoka, Y. Iriyama, T. Abe, M. Matsuoka, Z. Ogumi, *J. Power Sources*, **150**, 27 (2005).
4. M. L. Perry, T. F. Fuller, *J. Electrochem. Soc.*, **149**, S59 (2002).
5. C. Bianchini, P. K. Shen, *Chem. Rev.*, **109**, 4183 (2008).
6. L. An, T. S. Zhao, J. B. Xu, *Int. J. Hydrogen Energy*, **36**, 13089 (2011).
7. L. An, Z. H. Chai, L. Zeng, P. Tan, T. S. Zhao, *Int. J. Hydrogen Energy*, **38**, 14067 (2013).
8. L. An, R. Chen, *J. Power Sources*, **329**, 484 (2016).
9. K. Matsuoka, Y. Iriyama, T. Abe, M. Matsuoka, Z. Ogumi, *J. Electrochem. Soc.*, **152**, A727 (2005).
10. T. M. Brueckner, E. Wheeler, B. Chen, E. N. E. Sawy, P. G. Pickup, *J. Electrochem. Soc.*, **166**, F942 (2019).
11. B. Beden, I. Cetin, A. Kahyaoglu, D. Takky, C. Lamy, *J. Catal.*, **104**, 37 (1987).
12. Y. Kwon, S. C. S. Lai, P. Rodriguez, M. T. M. Koper, *J. Am. Chem. Soc.*, **133**, 6914 (2011).
13. M. S. Ureta-Zanartu, A. Alarcon, G. Munoz, C. Gutiérrez, *Electochim. Acta*, **52**, 7857 (2007).
14. L. Xin, Z. Zhang, J. Qi, D. Chadderdon, W. Li, *Appl. Catal. B*, **125**, 85 (2012).
15. D. Huang, Y. Luo, S. Li, M. Wang, Y. Shen, *Electrochim Acta*, **174**, 933 (2015).
16. X. Zhang, X. Wang, L. Le, A. Ma, S. Lin, *J. Mater. Chem. A*, **3**, 19273 (2015).
17. F. Papiya, A. Nandy, S. Mondal, P. P. Kundu, *Electrochim. Acta*, **254**, 1 (2017).
18. E. N. Alvar, B. Zhou, S. H. Eichhorn, *J. Mater. Chem. A*, **17**, 6540 (2016).
19. J. Liu, L. Jiang, T. Zhang, J. Jin, L. Yuan, G. Sun, *Electrochim. Acta*, **205**, 38 (2016).
20. X. Lv, W. Lv, X. Zheng, C. Zhang, L. Zhi, Q. H. Yang, *Chem. Commun.*, **51**, 3911 (2015).
21. H. Y. Y. Ko, M. Mizuhata, A. Kajinami, S. Deki, *J. Electroanal. Chem.*, **559**, 91 (2003).
22. S. Yongprapat, A. Therdthianwong, S. Therdthianwong, *J. Electroanal. Chem.*, **697**, 46 (2013).
23. D. Van Dao, G. Adilbish, T. Duc Le, T. T. D. Nguyen, I. H. Lee, Y. T. Yu, *J. Catal.*, **377**, 589 (2019).

24. H. Gao, Y. Cao, Y. Chen, et al., *J. Alloys Compd.*, **732**, 460 (2018).

25. L. Karuppasamy, C. Y. Chen, S. Anandan, J. J. Wu, *Electrochim. Acta*, **246**, 75 (2017).

26. I. Kaskow, P. Decyk, I. Sobczak, *Appl. Surf. Sci.*, **444**, 197 (2018).

27. V. Kepenienė, R. Stagniūnaitė, L. Tamašauskaitė-Tamašiūnaitė, et al., *Mat. Chem. Phys.*, **241** (2020).

28. N. Ostojic, Z. Duan, A. Galyamova, G. Henkelman, R. M. Crooks, *J. Am. Chem. Soc.*, **140**, 13775 (2018).

29. V. Kepenienė, L. Tamašauskaitė-Tamašiūnaitė, J. Vaičiūnienė, R. Kondrotas, V. Pakštas, E. Norkus, *Mater. Sci.*, **22**, 243 (2016).

30. M. M. Yusuf, A. B. Radwan, R. A. Shakoor, et al., *J. Appl. Electrochem.*, **48**, 391 (2018).

31. J. Yang, X. Tan, Y. Qian, et al., *J. Appl. Electrochem.*, **46**, 779 (2016).

32. S. Štrbac, I. Srejic, Z. Rakočevic, *J. Electroanal. Chem.*, **789**, 76 (2017).

33. J. Yang, J. Wang, L. Zhu, W. Zeng, J. Wang, *Mater. Lett.*, **234**, 331 (2019).

34. K. M. Shi, X. Cheng, Z. Y. Jia, J. W. Guo, C. Wang, J. Wang, *Int. J. Hydrogen Energy*, **41**, 16903 (2016).

35. J. C. Fuggle, E. Kallne, L. M. Watson, D. J. Fabian, *Phys. Rev. B*, **16**, 750 (1977).

36. C. Battistoni, G. Mattogno, R. Zanoni, L. J. Naldini, *Electron. Spectrosc. Relat. Phenom.*, **28**, 23 (1982).

37. P. T. Hsieh, Y. C. Chen, K. S. Kao, C. M. Wang, *Appl. Phys. A*, **90**, 317 (2008).

38. L. Wang, L. Zhuang, H. Xin, Y. Huang, D. Wan, *Open J. Inorg. Chem.*, **5**, 12 (2015).

39. E. Beche, P. Charvin, D. Perarnau, S. Abanades, G. Flamant, *Surf. Interf. Anal.*, **40**, 264 (2008).

40. H. K. Jeong, E. Echeverria, P. Chakraborti, H. T. Le, P. A. Dowben, *RSC Adv.*, **7**, 10968 (2017).

41. Y. Zhu, M. Yue, V. Natarajan, et al., *RSC Adv.*, **8**, 14879 (2018).

42. H. Angerstein-Kozlowska, B. E. Conway, A. Hamelin, L. Stoicoviciu, *Electrochim. Acta*, **31**, 1051 (1986).

43. Y. Zhao, L. Zhan, J. Tian, S. Nie, Z. Ning, *Electrochim. Acta*, **56**, 1967 (2011).

44. H. Qin, H. H. Yang, X. S. Zhang, P. Li, C. Mab, *Int. J. Hydrogen Energy*, **35**, 7667 (2010).

45. U. Paulus, T. Schmidt, H. Gasteiger, R. Behm, *J. Electroanal. Chem.*, **495**, 134 (2001).

46. C. Song, J. Zhang, in: *PEM Fuel Cell Electrocatalysts and Catalyst Layers*, Springer, London (2008).

47. X. Ge, A. Sumboja, D. Wuu, et al., *ACS Catal.*, **5**, 4643 (2015).

48. L. Karuppasamya, C. Chena, S. Anandanc, J. Wub, *Catal. Today*, **307**, 308 (2018).

49. C. Jin, J. Zhu, R. Dong, Q. Huo, *Electrochim. Acta*, **190**, 829 (2016).

50. C. Jin, C. Sun, R. Dong, Z. Chen, *Electrochim. Acta*, **56**, 321 (2010).

Virginija Kepenienė, Raminta Stagniūnaitė, Daina Upskuvienė, Loreta Tamašauskaitė-Tamašiūnaitė, Vidas Pakštas, Audrius Drabavičius, Mindaugas Andrulevičius, Eugenijus Norkus

AuCeO$_2$/C ELEKTROKATALIZINIŲ SAVYBIŲ ĮTAKA ETILENGLIKOLIO OKSIDACIJOS IR DEGUONIES REDUKCIJOS REAKCIJOMS

S a n t r a u k a

Tirtas elektrokatalizinis AuCeO$_2$/C ir Au/C katalizatorių aktyvumas etilenglikolio oksidacijos ir deguonies redukcijos reakcijoms. Minėti katalizatoriai buvo gauti adsorbcijos būdu, nusodinant aukso nanodaleles (AuNPs) ant cerio (IV) oksido / anglies (CeO$_2$/C) ir grynos anglies (C) pagrindų iš koloidinio aukso tirpalo. Ant abiejų naudotų pagrindų nusodintos apie 50 nm dydžio AuNPs.

Nustatyta, kad AuCeO$_2$/C katalizatorius pasižymi didesniu elektrokataliziniu aktyvumu tirtose etilenglikolio oksidacijos ir deguonies redukcijos reakcijose, palyginti su Au/C katalizatoriumi. Etilenglikolio oksidacijos metu AuCeO$_2$/C katalizatorius rodė apie tris kartus didesnes srovės tankio vertes, palyginti su Au/C katalizatoriumi. Deguonies redukcija naudojant AuCeO$_2$/C katalizatorių prasideda esant teigiamesnėms elektrodo potencialo vertėms nei su Au/C katalizatoriumi. Be to, išmatuotos kinetinės-difuzinės srities srovės tankio vertės taip pat yra didesnės naudojant pastarąjį elektrodą.

AuCeO$_2$/C katalizatoriaus aktyvumas siejamas su sinergetine sąveika tarp Au nanodalelių ir CeO$_2$. Gauti rezultatai leidžia manyti, kad šiomis sąlygomis gautas AuCeO$_2$/C katalizatorius yra tinkamesnis atliekant etilenglikolio oksidacijos tyrimus.